Confinement-induced InAs/GaSb heterojunction electron–hole bilayer tunneling field-effect transistor

J. L. Padilla, C. Medina-Bailon, C. Alper, F. Gamiz, and A. M. Ionescu

Citation: Appl. Phys. Lett. **112**, 182101 (2018); doi: 10.1063/1.5012948
View online: https://doi.org/10.1063/1.5012948
View Table of Contents: http://aip.scitation.org/toc/apl/112/18
Published by the American Institute of Physics

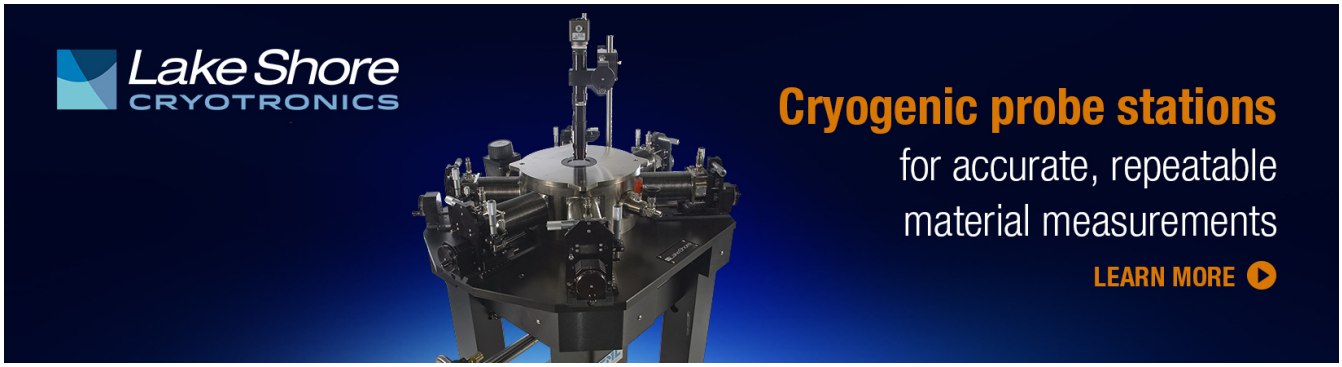

Confinement-induced InAs/GaSb heterojunction electron–hole bilayer tunneling field-effect transistor

J. L. Padilla,[1,a)] C. Medina-Bailon,[2] C. Alper,[3] F. Gamiz,[1] and A. M. Ionescu[3]
[1]*Departamento de Electrónica y Tecnología de los Computadores. Universidad de Granada. Avda. Fuentenueva s/n, 18071 Granada, Spain*
[2]*Device Modelling Group. University of Glasgow. Glasgow G12 8QQ, Scotland*
[3]*Nanoelectronic Devices Laboratory, École Polytechnique Fédérale de Lausanne, Lausanne CH-1015, Switzerland*

(Received 9 November 2017; accepted 14 April 2018; published online 30 April 2018)

Electron–Hole Bilayer Tunneling Field-Effect Transistors are typically based on band-to-band tunneling processes between two layers of opposite charge carriers where tunneling directions and gate-induced electric fields are mostly aligned (so-called line tunneling). However, the presence of intense electric fields associated with the band bending required to trigger interband tunneling, along with strong confinement effects, has made these types of devices to be regarded as theoretically appealing but technologically impracticable. In this work, we propose an InAs/GaSb heterostructure configuration that, although challenging in terms of process flow design and fabrication, could be envisaged for alleviating the electric fields inside the channel, whereas, at the same time, making quantum confinement become the mechanism that closes the broken gap allowing the device to switch between OFF and ON states. The utilization of induced doping prevents the harmful effect of band tails on the device performance. Simulation results lead to extremely steep slope characteristics endorsing its potential interest for ultralow power applications. *Published by AIP Publishing.*
https://doi.org/10.1063/1.5012948

Electron–Hole Bilayer Tunneling Field-Effect Transistors (EHBTFETs) were originally proposed[1] aiming to exploit the benefits of dimensionality for band-to-band tunneling (BTBT) between 2-D electron and hole gases.[2] They were also conceived to profit from the advantages of line tunneling (BTBT direction aligned with the gate-induced electric field) versus point tunneling (both directions mutually perpendicular) controlling the band bending processes giving rise to the interband tunneling phenomena.[3,4] In order to keep a better electrostatic control on the channel and prevent DOS tails inside the gap, the highly populated electron and hole layers inside the channel were engineered so that they were formed by an appropriate workfunction choice and/or gate biasing.

However, it was systematically argued that due to size and bias-induced quantization issues, EHBTFETs would require prohibitively high voltages leading to unacceptably high electric fields, causing oxide reliability concerns.[5] Moreover, the consideration of quantum confinement effects showed the appearance of parasitic diagonal leakage tunneling between regions with different degrees of quantization.[6] To overcome this parasitic leakage, a heterogate EHBTFET (HG-EHBTFET) was proposed,[6] along with a solution to alleviate the large electric fields through the utilization of asymmetric configurations[7] and pseudo-bilayer structures.[8]

Notwithstanding the foregoing solutions that showed improved performance, there was still the issue of low ON current levels reported from indirect materials like germanium. In this work, we propose an EHBTFET based on an ultrathin body (UTB) InAs/GaSb single channel. Experimental UTB InAs/GaSb bilayers on silicon were investigated for single structure CMOS.[9] Simulation results for our proposed device feature electric fields below the typical levels traditionally associated with EHBTFETs along with the advantages of the utilization of direct tunneling materials. Moreover, the most interesting particularity of this device is that, considering the band structure parameters of InAs and GaSb,[10] this device would not allow the switching between OFF and ON states without the interplay of quantum confinement effects given that, semiclassically, the conduction band of InAs and the valence band of GaSb would always have a certain energy overlap. It is important to notice that, although the idea of closing the broken gap at the InAs/GaSb heterojunction by means of quantum confinement effects is not new,[11] our proposal of InAs/GaSb EHBTFET allows us to avoid the utilization of p+ doped GaSb layers as done so far[11,12] and the subsequent risk of band tails associated with high doping concentrations.

The analyzed device structure is depicted in Fig. 1. It features a p^+ GaSb source region (10^{19} acceptors/cm^3), an intrinsic GaSb bottom channel region (10^{15} acceptors/cm^3), an intrinsic InAs top channel region (10^{15} donors/cm^3), and an n-doped InAs drain region (10^{19} donors/cm^3). Top and bottom gate dielectrics are 3 nm-thick HfO_2 layers. Two HfO_2 spacers have been placed at the top left side and bottom

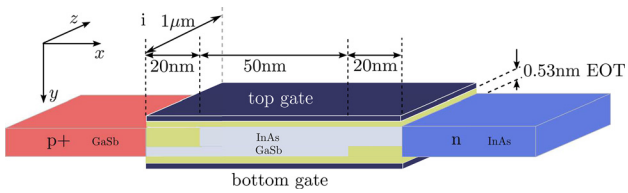

FIG. 1. Schematic representation (not to scale) of the InAs/GaSb Heterostructure EHBTFET considered in this work. Top left and bottom right HfO_2 spacers in the channel prevent parasitic source-to-channel and channel-to-drain BTBT from degrading the switching performance of the device.

a)Electronic mail: jluispt@ugr.es

right side of the channel with thicknesses equal to t_{InAs} and t_{GaSb}, respectively, to avoid parasitic source-to-channel and channel-to-drain BTBT. Top and bottom gate workfunctions are chosen to be $\phi_{tg} = 4.4\,eV$ and $\phi_{bg} = 5\,eV$ and play an important role so that subband alignment can take place with no bottom gate bias applied, $V_{BG} = 0V$, and very low top gate voltage, V_{TG}. Although the device structure representation in Fig. 1 is 3D for a better perception of the proposed design, the results presented throughout our work correspond to simplified 2D simulations where the transport occurs in the x-direction.

The InAs layer thickness determines the size-induced confinement strength at the top of the channel and thus the separation between the forbidden edge of the conduction band and its first subband. In principle, the strong quantization ensued from the extremely reduced InAs electron effective mass, $m_e(\Gamma) = 0.023m_0$, would make impractical the subband alignment between InAs and GaSb at low V_{TG} biases for ultra-thin InAs slabs like those reported in experimental works[9] with InAs/GaSb stacks reaching 2.5 nm for the InAs film. Nevertheless, the reduction in the thickness of the InAs layer combined with its well-known nonparabolic behavior causes an increase in the electron effective mass that alleviates the strength of confinement. Most frequently, only the effective mass rise in the transport direction proves to be of interest; but in our case, we also need its variation in the direction of confinement for solving the Schrödinger equation employing the effective mass approximation (EMA). In Table I, we list the values of $m_e(\Gamma)$ that we will use in our simulations for both transport and confinement directions estimated by tight-binding (TB) as a function of film thickness.[13] Notice how the growing effect on the effective masses is significantly more relevant for the confinement direction.

The heavy hole effective mass for GaSb ($m_{hh} = 0.4m_0$) results in weaker confinement effects at the bottom of the channel compared to the aforementioned situation at the upper slab. Yet, it was demonstrated that in III-V compounds, the top of the valence band is connected with the conduction band through an imaginary branch with lower mass[14] (approximately equal to that of light holes, m_{lh}[15]) even in the presence of strong quantization effects. In practical terms, this means that the tunneling effective mass to be used for the contribution to BTBT from heavy hole subbands will be the one corresponding to light holes, i.e., $m_{hh,imag} \approx m_{lh}$. This anti-crossing[16] of the light hole and heavy hole branches will be beneficial for the resulting I_{DS} levels as lower masses provide higher tunneling currents.

The simulation approach followed in this work differs from that reported in others[6–8] where a two-step setup integrating the TCAD simulator Silvaco ATLAS (v.5.20.2.R)[17] and Synopsys Sentaurus (v.2014.09)[18] treated BTBT as a postprocessing phenomenon. That approach worked well as long as the total injected charge via BTBT turned out to be negligible compared to the total charge distribution obtained in the absence of tunneling by solving in a self-consistent way the Schrödinger and Poisson equations employing the effective mass approximation.[15,19,20] However, in our proposed device, the utilization of direct materials in which BTBT is not mediated by phonons provides significantly higher levels of tunneling charge, which makes the aforementioned two-step simulation layout not suitable for our aim. Therefore, our simulation approach will entirely make use of Synopsys Sentaurus with an additional customization inside it which allows us to incorporate subband discretization in a self-consistent way. To do so, we modify the so-called *Apparent Band-Edge Shift Model*, which is a user customizable model included in the physical model interface (PMI) of Sentaurus for bandgap editing through appropriate C++ functions. By doing so, the so far semiclassical edges of the conduction and valence bands are readjusted to make them coincident with their first subbands[21] so that BTBT can take place between bound states and not between quantum mechanically forbidden states. BTBT is accounted for by means of the dynamic nonlocal BTBT model of Sentaurus, which dynamically calculates the tunneling paths based on the energy band profiles.

TABLE I. Electron effective masses corresponding to the Γ-valley in transport and confinement directions, $m_{e,x}(\Gamma)$ and $m_{e,y}(\Gamma)$, for different InAs thicknesses. Interpolated values from those herein displayed will be used in our work.

InAs layer thickness	$m_{e,x}(\Gamma)$	$m_{e,y}(\Gamma)$	$\alpha(eV^{-1})$	$m_{e,bulk}(\Gamma)$
10 nm	0.033	0.043		
7 nm	0.038	0.055		
5 nm	0.047	0.068	2.6	0.023
3 nm	0.066	0.102		
2 nm	0.086	0.155		

The band profile along a vertical cut taken at the center of the device for $t_{InAs} = 3.5$ nm and $t_{GaSb} = 4$ nm is shown in Fig. 2 for $V_{TG} = 0$ and $V_{TG} = 0.2\,V$ with $V_{DS} = 0.2V$. We have displayed in both cases the semiclassical edges of the conduction and valence bands to illustrate that in the absence of subband discretization, the switching ability of the device would be suppressed since BTBT would always be enabled due to the existing energy overlap between bands resulting from the InAs/GaSb broken gap junction. On the other hand, it is precisely the existence of quantum confinement which allows the broken gap to become staggered and thus opens the possibility for the proposed structure to become a feasible steep slope switch. As mentioned above, notice that the limiting factor will be the InAs layer thickness as it shows stronger quantization effects caused by the value of its electron effective mass. Quantum confinement for holes will also be considered due to the reduced thickness of the GaSb layer required to induce the doping at the bottom of the channel. Note that, in contrast to our work, hole confinement need not be considered in highly doped GaSb bulk devices like those so far reported in the literature.[11]

The main agent pushing away the first electron subband, E_{e1}, from the conduction band edge comes from size-induced confinement imposed by t_{InAs}. Therefore, it is a matter of making an adequate slab thickness choice so as to obtain the OFF state when $V_{TG} = 0V$. Figure 3 shows the top gate voltage at which first subbands align, $V_{TG,align}$, for different combinations of t_{InAs} and t_{GaSb}. Observe how, for a chosen value of $V_{TG,align}$, the effective mass increase in the confinement direction allows us to envisage thinner InAs films inside the channel. Once that the slab choice has been made ensuring that the broken gap is closed at $V_{TG} = 0V$, it is the turn of the bias-induced contribution to confinement through increasing values of V_{TG} —within the allowed range

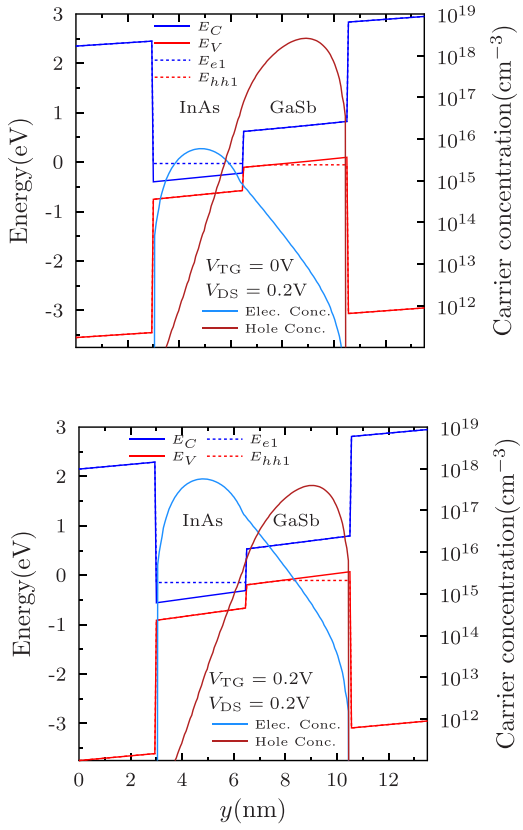

FIG. 2. Band profiles across a vertical cut taken at the center of the device for $t_{InAs} = 3.5$ nm and $t_{GaSb} = 4$ nm along with the corresponding quantized carrier concentrations. For $V_{TG} = 0$V (top), subband alignment has not been reached yet, in contrast to what happens for $V_{TG} = 0.2$V (bottom).

of V_{TG} ($0 < V_{TG} < V_{DD}$)—so that E_{e1} is lowered till the moment when alignment with the first GaSb heavy hole subband, E_{hh1}, is attained. This alignment is achievable by applying positive V_{TG} values, provided that the top gate efficiency (mathematically defined as dE_{e1}/dV_{TG}) is negative, as seen in Fig. 4 (left axis), indicating that the bigger the

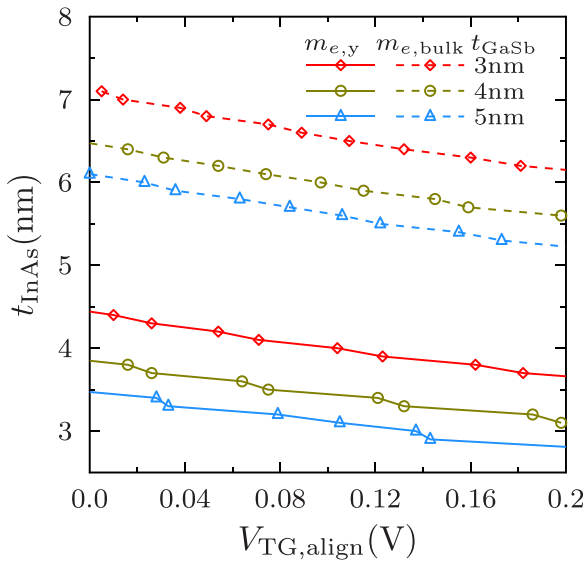

FIG. 3. Impact of the InAs layer thickness variation on the top gate voltage at which first subbands align, $V_{TG,align}$, due to the resulting electron effective mass variation in the confinement direction. $V_{DS} = 0.2$V.

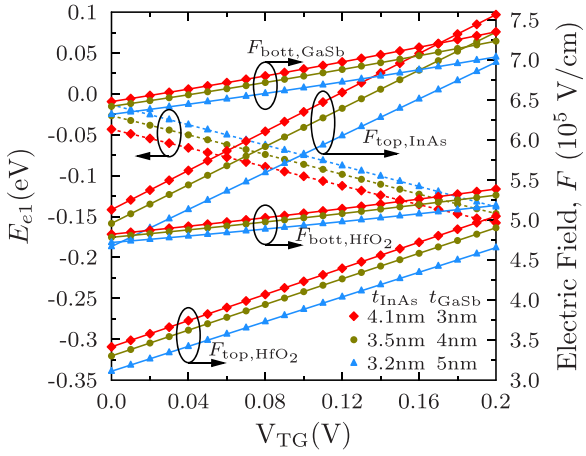

FIG. 4. (Left axis) Dependence of the first electron subband vs. V_{TG} for different InAs and GaSb thicknesses showing a negative value of $dE_{e1}/dV_{TG} \approx -0.5$. (Right axis) Electric field values at the top and bottom sides of the channel. $V_{DS} = 0.2$V.

V_{TG}, the lower the E_{e1} in the InAs layer. Absolute values of the top gate efficiency extracted from Fig. 4 prove to be ≈ 0.5, being consistent with the reported effect[22] of quantum confinement making the gate efficiencies lie considerably below 1 for bilayer TFETs.

The electric fields at the channel-to-dielectric interfaces at the center of the device are shown in Fig. 4 (right axis) featuring reduced values compared to those traditionally obtained for ultrathin bilayer TFETs and remaining below the breakdown levels for HfO_2 that usually lie over 10^6 V/cm.[23] We have displayed the electric fields at both sides of the interface: inside the oxide (F_{bott,HfO_2}, F_{top,HfO_2}) and inside the channel ($F_{bott,GaSb}$, $F_{top,InAs}$). Figure 5 (top) shows the transfer characteristics of the proposed InAs/GaSb Heterostructure EHBTFET corresponding to $t_{GaSb} = 3, 4, 5, 6, 7$ nm, adjusting in each case the InAs slab thickness so that $V_{TG,align} \approx 0.07$ V. It can be seen how, as mentioned before, the steep slope switching behavior is attainable, thanks to the size-induced subband discretization which suppresses BTBT in the OFF state by eliminating the semiclassical energy overlap between the conduction band in the InAs layer and the valence band in the GaSb layer. Variations of the InAs thickness for a fixed t_{GaSb} allow us to control the E_{e1} level and therefore to adjust the onset of BTBT at different values of V_{TG}. The fact that some of the displayed curves feature numerical convergence issues when current levels escalate is possibly due to the extremely reduced spatial region where BTBT takes place between both films. The maximum attainable currents for the affected curves might be inferred extrapolating their behavior from the points where the simulations start to fail converging. If we did so, their values would presumably range from $\approx 100\mu$A/μm (for $t_{GaSb} = 6$ nm) to $\approx 600\mu$A/μm (for $t_{GaSb} = 3$ nm) at $V_{TG} = V_{DS} = 0.2$V. Observe how slimming down the GaSb slab reveals itself as an appealing means to enhance the ON-state current. This happens because the thinner the GaSb layer, the stronger the confinement effects at the bottom of the channel, leading to lower energy levels for E_{hh1} and to shorter tunneling lengths between E_{e1} and E_{hh1} subbands.

The displayed I_{DS}–V_{TG} curves feature subthreshold swings ranging between 4 and 6 mV/dec over 7 decades of

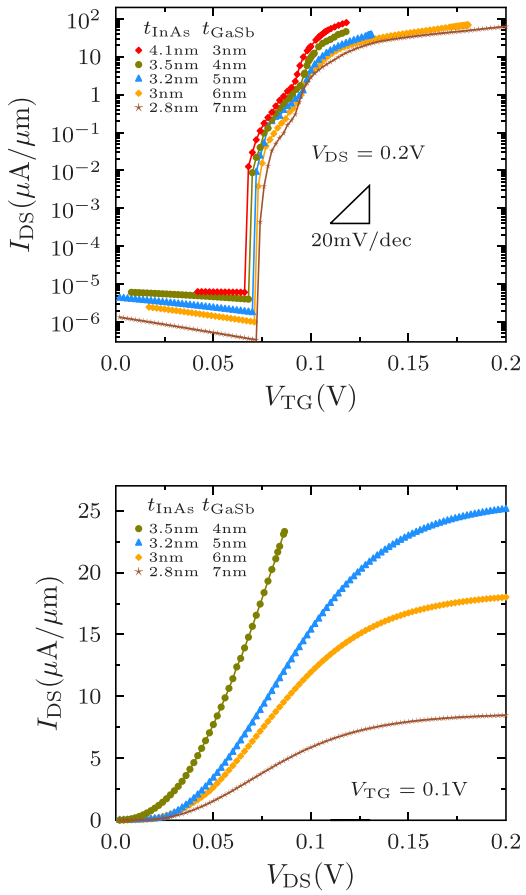

FIG. 5. (Top) Transfer characteristics of the InAs/GaSb Heterostructure EHBTFET with $t_{GaSb} = 3,4,5,6,7$ nm, along with the adequate selection of the InAs layer thickness inside the channel so that the V_{TG} value for the vertical BTBT onset takes place around 0.07V. (Bottom) Output characteristics corresponding to $V_{TG} = 0.1$V.

current with acceptable ON state levels for ultralow V_{DD} operation ($V_{TG} = V_{DS} = V_{DD} = 0.2$V). The reason for the apparent kink located around $V_{TG} \approx 0.09$ V comes from the fact that the quantization strength inside the GaSb film proves to be different when this layer is sandwiched by HfO_2 and InAs (center of the channel) or entirely by HfO_2 (left side of the channel). As a result of this, the E_{hh1} subband lies slightly above in the left side, and therefore, the first BTBT events are triggered when ramping V_{TG} is diagonal from the bottom left side of the channel to the top center. When vertical BTBT arises a bit later in the center of the channel, the current is boosted due to the associated shorter tunneling lengths. Overall, the appealing behavior reported in the subthreshold region must be understood in the appropriate context, which is that of an ideal scenario where potential sources of degradation such as tunneling leakage through the gates or the appearance of native oxide species at the high-κ/III-V interface have not been considered. The rationale behind such a choice, at a first stage of analysis of the proposed device, is to assess its optimal behavior and to evaluate its best expectable degree of performance.

In Fig. 5 (bottom), we present the output characteristics of the analyzed device taking the adjusted values for the different slab thicknesses. V_{TG} has been fixed to 0.1 V and not to 0.2 V due to the lack of numerical convergence encountered when the current values scaled above a certain level as mentioned above. In any case, for $t_{GaSb} \leq 4$ nm, the numerical issues still remain. The displayed curves that are complete show the expected transition between a superlinear regime and a saturation region where the thinner the channel, the higher the drain current attained.

A last consideration should also be made with respect to the potential impact associated with the mobility reduction entailed by the increasing effect of the interface roughness scattering when the channel thickness is scaled down. In Fig. 6, we show the variation of the transfer and output characteristics for a conservative mobility of 5×10^3 cm^2/Vs according to experimental results from InAs/GaSb quantum well structures.[24] It can be seen how the steepness of the subthreshold slope is not affected by the mobility decrease as it is mainly conditioned by the BTBT phenomena. However, the ON-state current levels show a certain reduction that might be estimated to be around 20% for the aforementioned mobility value at 300 K.

In this work, we have proposed an InAs/GaSb heterostructure EHBTFET that utilizes the subband quantization ensued from size-induced confinement as the mechanism that closes the broken gap at the InAs/GaSb heterojunction and blocks the otherwise always enabled vertical band-to-band tunneling. The presence of induced doping profiles inside the channel due to the utilization of an electron-hole bilayer structure prevents the band tails associated with heavily doped materials. We have shown that an appropriate slab thickness choice makes the device behave as a steep slope

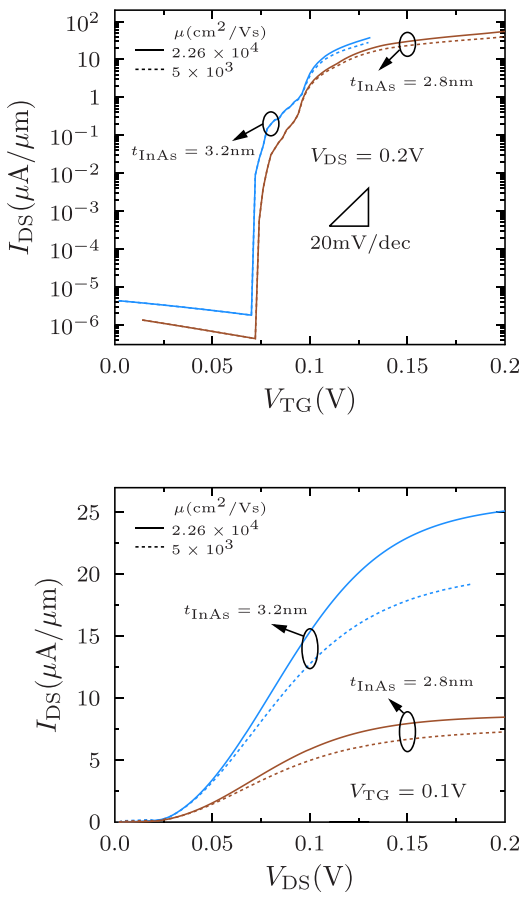

FIG. 6. Effect of the mobility reduction on the transfer (top) and output (bottom) characteristics of the InAs/GaSb Heterostructure EHBTFET.

switch suitable for ultralow power applications with simulated ON current levels comparable to experimental results from InAs/GaSb TFETs[11] with highly doped substrates.

This research received funding from the European Community's Seventh Framework Programme Marie Curie Action under grant agreement No. 291780 (Andalucia Talent Hub) and from the Spanish Ministry of Economy (TEC2014-59730-R).

[1]L. Lattanzio, L. De Michielis, and A. M. Ionescu, Solid-State Electron. **74**, 85 (2012).
[2]S. Agarwal and E. Yablonovitch, in *69th Annual Device Research Conference* (2011), pp. 199–200.
[3]Y. Lu, G. Zhou, R. Li, Q. Liu, Q. Zhang, T. Vasen, S. D. Chae, T. Kosel, M. Wistey, H. Xing, A. Seabaugh, and P. Fay, IEEE Electron Device Lett. **33**, 655 (2012).
[4]M. Schmidt, A. Schäfer, R. A. Minamisawa, D. Buca, S. Trellenkamp, J. M. Hartmann, Q. T. Zhao, and S. Mantl, IEEE Electron Device Lett. **35**, 699 (2014).
[5]A. Revelant, A. Villalon, Y. Wu, A. Zaslavsky, C. Le Royer, H. Iwai, and S. Cristoloveanu, IEEE Trans. Electron Devices **61**, 2674 (2014).
[6]J. L. Padilla, C. Alper, F. Gamiz, and A. M. Ionescu, Appl. Phys. Lett. **105**, 082108 (2014).
[7]J. L. Padilla, C. Alper, A. Godoy, F. Gamiz, and A. M. Ionescu, IEEE Trans. Electron Devices **62**, 3560 (2015).
[8]J. L. Padilla, C. Alper, C. Medina-Bailon, F. Gamiz, and A. M. Ionescu, Appl. Phys. Lett. **106**, 262102 (2015).
[9]M. Yokoyama, H. Yokoyama, M. Takenaka, and S. Takagi, in *2014 Symposium on VLSI Technology* (2014), pp. 1–2.
[10]I. Vurgaftman, J. R. Meyer, and L. R. Ram-Mohan, J. Appl. Phys. **89**, 5815 (2001).
[11]G. Zhou, R. Li, T. Vasen, M. Qi, S. Chae, Y. Lu, Q. Zhang, H. Zhu, J.-M. Kuo, T. Kosel, M. Wistey, P. Fay, A. Seabaugh, and H. Xing, in *International Electron Devices Meeting* (2012), Vol. 4, pp. 32.6.1–32.6.4.
[12]C.-Y. Hsu, C.-Y. Chang, E. Chang, and C. Hu, IEEE J. Electron Devices Soc. **4**, 60 (2016).
[13]G. Mugny, F. Triozon, J. Li, Y.-M. Niquet, G. Hiblot, D. Rideau, and C. Delerue, in *Proceedings of EUROSOI-ULIS* (2015), pp. 301–304.
[14]A. Pan and C. Chui, J. Appl. Phys. **116**, 054509 (2014).
[15]C. Alper, M. Visciarelli, P. Palestri, J. L. Padilla, A. Gnudi, E. Gnani, and A. M. Ionescu, in *Proceedings of SISPAD* (2015), pp. 273–276.
[16]S. Jin, A.-T. Pham, W. Choi, Y. Nishizawa, Y.-T. Kim, K.-H. Lee, Y. Park, and E. Jung, in *IEEE International Electron Devices Meeting* (2014), pp. 7.5.1–7.5.4.
[17]ATLAS Users Manual (Silvaco, 2014).
[18]Sentaurus Device Tool Manual, v. J-2014.09 (Synopsys, 2014).
[19]A. M. Walke, A. S. Verhulst, A. Vandooren, D. Verreck, E. Simoen, V. R. Rao, G. Groeseneken, N. Collaert, and A. V. Y. Thean, IEEE Trans. Electron Devices **60**, 4057 (2013).
[20]C. Alper, L. Lattanzio, L. De Michielis, P. Palestri, L. Selmi, and A. M. Ionescu, IEEE Trans. Electron Devices **60**, 2754 (2013).
[21]S. Sant and A. Schenk, IEEE Trans. Electron Devices **63**, 2169 (2016).
[22]J. T. Teherani, S. Agarwal, E. Yablonovitch, J. L. Hoyt, and D. A. Antoniadis, IEEE Electron Device Lett. **34**, 298 (2013).
[23]D. Wheeler, A. Seabaugh, L. Froberg, C. Thelander, and L.-E. Wernersson, in International Semiconductor Device Research Symposium (2007).
[24]W. Huang, W. Ma, J. Huang, Y. Zhang, Y. Cao, C. Zhao, and X. Guo, Solid State Commun. **267**, 29 (2017).